

# Geometry optimization of a heat storage system for concentrated solar power plants (CSP)

Aran Solé <sup>a,\*</sup>, Quentin Falcoz <sup>b</sup>, Luisa F. Cabeza <sup>c</sup>, Pierre Neveu <sup>b</sup>

<sup>a</sup> Department of Mechanical Engineering and Construction, Universitat Jaume I, Campus del Riu Sec s/n, 12071 Castelló de la Plana, Spain

<sup>b</sup> University of Perpignan/PROMES-CNRS, Rambla de la thermodynamique, Tecnosud, 66100, Perpignan, France

<sup>c</sup> GREiA Research Group, INSPIRES Research Centre, Universitat de Lleida, Pere de Cabrera s/n, 25001, Lleida, Spain

## ARTICLE INFO

### Article history:

Received 26 October 2017

Received in revised form

9 January 2018

Accepted 1 February 2018

### Keywords:

Thermal energy storage (TES)  
Concentrated solar power plant (CSP)  
Phase change material (PCM)  
Constructural  
Exergy  
Optimization

## ABSTRACT

In the present study, geometry optimization of a phase change material (PCM) heat storage system is presented. The existing PCM-fins heat exchanger system works at the back side of a solar receiver in order to minimize the effect of the solar radiation fluctuations inside the cavity. As initially designed, the system does not accomplish the expected design purposes and thus optimization is needed. Optimization is usually time-consuming and some algorithms need a starting point, therefore one suitable method is geometrical optimization which aims to find the optimal shape of a system for a given criteria and providing a rough optimal geometry. Here, constructal theory, 'point to volume', is applied to find the optimum shape factor of the elemental volume of the presented PCM-heat exchanger. With this methodology, an optimum ratio of the PCM and fin width and length is found and beyond that the method is extended to 'surface to volume' problem. Results have been numerically validated using a CFD software and demonstrate that it gives a very good approximation of the real optimum which can be used as initial configuration for further optimization through CFD simulation or other optimization methods that require a starting point.

© 2018 Elsevier Ltd. All rights reserved.

## 1. Introduction

Electricity consumption is growing rapidly in many countries; its global use increased by 54% between 1990 and 2005. Nowadays, electricity is the second major energy commodity in OECD countries with a share of 22%, after oil products with a 47% [1]. To move towards depletion of fossil fuels consumption to achieve the worldwide goals of climate change and CO<sub>2</sub> mitigations, the use of renewable energies is essential.

One feasible way to produce electricity from renewable energy is concentrated solar power (CSP) plants [2,3]. By 2050, with appropriate support, CSP could provide 11.3% of global electricity, with 9.6% from solar power and 1.7% from backup fuels (fossil fuels or biomass) [2]. Nowadays, four CSP technologies are represented at pilot and commercial scale: parabolic-trough collectors (PTCs), linear Fresnel reflector (LFR) systems, power towers or central receiver systems (CRS), and dish/engine systems (DE) [4]. According to Lovegrove et al. [5] tower systems or central receiver systems

represent the next generation of CSP plants as they can achieve higher efficiency and lower cost.

To compensate the intermittency of solar resource and to protect the solar receiver of a central receiver system, thermal energy storage technologies can be employed. Among these technologies, phase change materials (PCM) tanks can either be implemented for continuous electricity production, by supplying required heat when sun is not available [6,7], or to protect the receivers in tower system [8,9]. In parallel, other more mature technologies, mainly based on solar salts, for CSP applications are being tested at pilot plant scale [10] and on the other hand first demonstrations at pilot plant scale of more recent technologies, based on thermochemical materials, are growing [11,12].

In the literature, publications regarding design and optimization of PCM heat exchanger for storage in CSP applications can be found [13,14]. Several technologies have been investigated: encapsulated PCM for thermochemical systems [15–17], shell and tube heat exchangers [18–20] implementing finned tubes [21,22], heat pipes [23] or metallic foam [24] for heat transfer enhancement. All these studies make extensively use of CFD tools, permitting accurate performance evaluation through 2D or 3D modelling. However,

\* Corresponding author.

E-mail address: [sole@uji.es](mailto:sole@uji.es) (A. Solé).

Nomenclature		Greek symbols	
c	heat capacity J kg <sup>-1</sup> K <sup>-1</sup>	$\beta$	kinetics constant K <sup>-1</sup> s <sup>-1</sup>
d	height of the conductive material m	$\theta$	Carnot factor
exd	total exergy destruction W	$\rho$	density kg. m <sup>-3</sup>
f	shape factor	$\sigma_q$	Heat source W m <sup>-3</sup>
H	height of the system m	$\phi$	liquid fraction
jq	heat flux density W m <sup>-2</sup>	$\varphi$	Conductive to total volume ratio
k	thermal conductivity W m <sup>-1</sup> K <sup>-1</sup>		
$\bar{k}$	conductivities ratio	Subscript	
L	length of the system m	0	elemental (geometry) or reference (temperature)
Lm	latent heat J kg <sup>-1</sup>	1	construct 1
$\dot{Q}$	total heat power W	a	active material
$\bar{q}_X$	average heat flux to reach x W	c	conductive material
S	total entropy production W K <sup>-1</sup>	Cu	copper
T	temperature K	irr	irreversible
$\bar{T}$	average temperature K	m	melting
tX	time to reach x s	PCM	phase change material
W	width of the system m	ptv	point to volume
X	conversion degree	stv	surface to volume
Z	exergy impedance W <sup>-1</sup>		
z	dimensionless exergy impedance	Superscript	
		*	optimal

such tools could be time consuming when optimizing. The geometry needs to be drawn at a first step before generating a mesh. Therefore, simplified tools to approach the optimized geometry could be very interesting. Optimization methods giving valuable results with relatively simple calculations and less time consuming are aimed for studying the plausibility of new systems. One method is geometrical optimization which aims to find the optimal shape of a system for a given criteria. Bejan proposed in 2000 [25], a general method devoted to this objective: the constructal theory [25]. Since then, several studies have been published proving the viability of this theory in a huge variety of fields, being one of them heat transfer and fluid flow systems [26]. In addition, and focusing on thermal energy storage designs, the constructal method has been extended to coupled heat and mass transfer by Azoumah et al. [27], or to thermochemical reactors, taking the total entropy production as minimization criteria [28]. Tescari et al. [29] revisited the so-called ‘point to volume’ problem (ptv) studied by Bejan in his original work [30], using the thermodynamic of irreversible processes. It was shown that global optimization gives better results than the step by step optimization usually used in the constructal theory. Moreover, this work defined the entropy and exergy impedances, which have to be minimised to facilitate heat transfer. Neveu et al. [31] successfully applied the impedance minimization method to thermochemical reactor.

The aim of the present study is to prove the fact that the impedance minimization gives a good approximation of the optimal shape of a defined geometry, and therefore it is an appropriate method to obtain a starting point for an accurate further optimization of TES systems predesign. Furthermore, this study introduces and solves an original problem, named ‘surface to volume’ (stv) problem, which represents a more realistic structure than the ptv problem for TES systems optimization.

## 2. Background

### 2.1. Protection storage for high temperature solar receiver

To smooth the variation of temperatures of a pressurized air

solar receiver of a concentrated solar plant (CSP) a PCM heat exchanger working between 873 K and 1173 K was designed and published by Verdier et al. [8,9]. The main idea of this PCM tank is to stabilize the outlet air temperature in case of cloud covering, as represented in Fig. 1 left, thus protecting the solar receiver and other critical downstream components. Fig. 1 right, shows the location of the PCM tank in the entire system being integrated at the back of the receiver.

The PCM used is lithium carbonate (Li<sub>2</sub>CO<sub>3</sub>) since its melting temperature is close to the working temperatures, being 996 K. The fins are made of copper, being a highly conductive metal. Pictures and a scheme of the current heat exchanger can be seen in Fig. 2. After tests, it was concluded that this heat exchanger needed to be optimized to achieve better results [9].

This study also provided a 2D model using CFD software. The PCM model is based on Calvet et al. study [32] in which the local liquid fraction ( $\phi$ ) evolution is evaluated through a 1st order heterogeneous kinetic law (Eqs. (1) and (2)):

$$\frac{d\phi}{dt} = \beta(T - T_m)\phi \text{ if } T < T_m \text{ (solidification conditions)} \quad (1)$$

$$\frac{d\phi}{dt} = \beta(T - T_m)(1 - \phi) \text{ if } T > T_m \text{ (melting conditions)} \quad (2)$$

The kinetic constant  $\beta$ , fitted by comparison between model and experiments, was found to be 0.001 K<sup>-1</sup> s<sup>-1</sup>. Verdier [33] also remarks that the value of  $\beta$  can have a big impact on computing time; however its effect to the TES evolution remains weak, showing that the behaviour of the PCM TES is controlled by heat transfer.

### 2.2. Geometrical optimization

Constructal theory initiated by Bejan [25] aims at optimizing the geometry of systems in which heat or matter is flowing. This method consists in finding the optimal geometrical shape that minimizes the global transfer resistance. Cooling of electronic devices was first investigated by Bejan [30] where also the ‘point to volume’ (ptv) problem was defined.

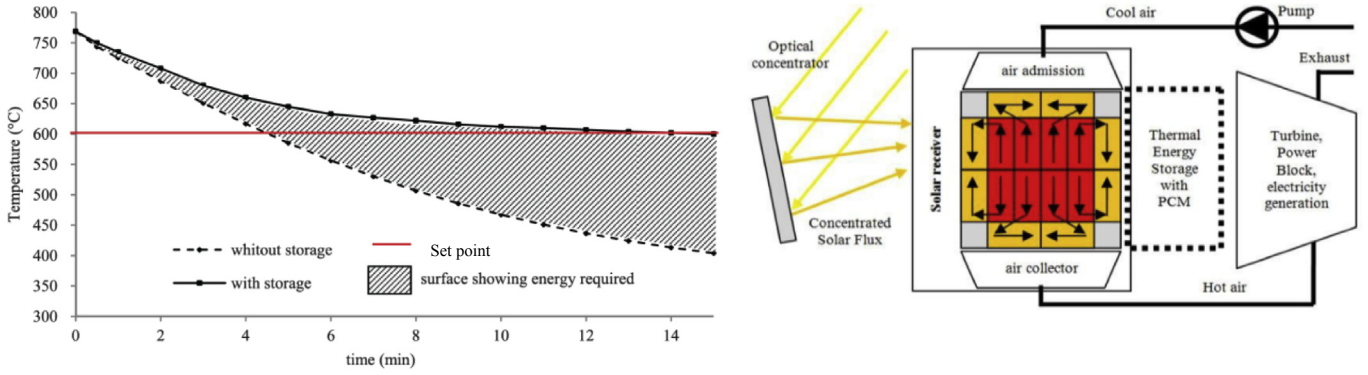


Fig. 1. Left: Expected effect on temperature with and without storage system, from Ref. [8]. Right: Scheme of the entire system and the PCM tank, from Ref. [9].

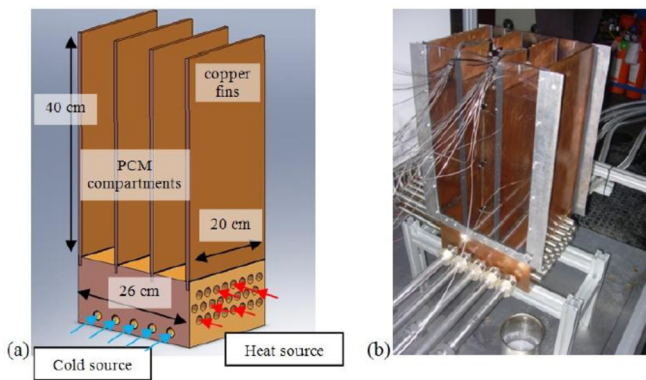


Fig. 2. PCM fins heat exchanger developed and tested for the solar receiver application [9].

In this paper, the system under study is composed of an active material releasing heat and a conductive path (Fig. 3). Surface (or volume) of both materials is given. Heat released by the active material is extracted through the fin(s) on the left side, maintained at  $T_0$ . All the other boundaries are thermally insulated. The constructal method consists in finding the optimal shape for the so-called elemental volume (Fig. 3a) (i.e. optimal shape factor  $H/L$  for a given conductive to active materials ratio  $d/H$ ), which minimizes the maximum temperature difference between the upper (or lower) right corner and the middle left point. Once the optimal elemental volume is found, the construct one device (Fig. 3b) is obtained by paving the given surface with optimal elemental

surfaces. The optimal number of elemental volumes is pursued using the same criterion. This process leads to find the optimal shape factor  $H_1/L_1$  and the optimal repartition of conductive material (i.e optimal ratios  $d_0/H_0$  and  $d_1/H_1$ ).

The constructal method was extended to coupled heat and mass transfer by Azoumah et al. [27] for solid-gas reactor design. This study shows that the optimal geometry deduced from the constructal theory leads to the maximum thermal power (i.e. highest kinetics) reachable for a solid/gas reactor. Following these studies, Tesdari et al. [29] revisited the pty problem by taking the total entropy production (or total exergy destruction) as minimization criterion, and performing a global optimization (i.e. each scale is optimized in a single step). It was shown that the total exergy destruction  $ex_d$  (W) could be expressed according to the generated heat power  $q$  (W) under the following remarkable form:

$$ex_d = Zq^2 \tag{3}$$

$Z$  is named exergy impedance. For the elemental volume (Fig. 3a), it writes:

$$Z_0 = \frac{1}{3k_cWT_0} \left( \frac{1}{\phi f} + \frac{\bar{k}}{4} f(1 - \phi) \right) \tag{4}$$

where

- $k_c$ : thermal conductivity of the conductive path ( $W.m^{-1}K^{-1}$ )
- $f = H/L$ : Shape factor
- $\phi = d/H$ : Conductive to total volume ratio

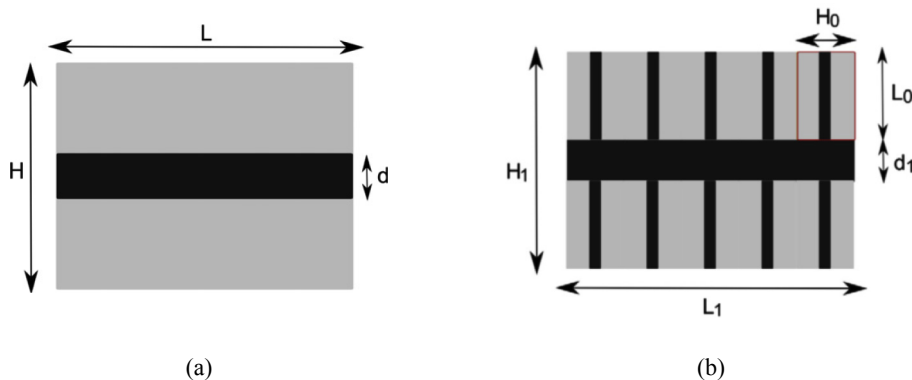


Fig. 3. (a) Elemental volume. (b) Construct 1 device with its optimized elemental volume represented in red, from Ref. [25].

$\tilde{k} = k_c/k_a$ : Conductivities ratio,  $k_a$  being the thermal conductivity of active material  
 $W$ : Width of the system (m)  
 $T_0$ : Constraint temperature taking as exergy reference temperature (K)

The minimization is then carried on the dimensionless impedance defined by:

$$z_0 = \frac{Z_0}{Z_c} = \frac{1}{\phi f} + \frac{\tilde{k}}{4} f (1 - \phi) \quad (5)$$

where  $Z_c = \frac{1}{3k_c W T_0}$

The optimal solution is:

$$f_0^* = 2 \left[ \tilde{k} \phi (1 - \phi) \right]^{-1/2} \quad (6)$$

Similar expressions have been derived for construct 1 system. Results have been validated by comparing the optimal configuration obtained from Eq. (6) with temperature fields computed using CFD simulations. Neveu et al. [31] extended this methodology to thermochemical reactors, coupling constructal theory ('point to volume' problem), exergy analysis, and thermodynamics of irreversible process. It permits to refine the solution proposed for thermochemical reactor formerly obtained by Azoumah et al. [27] by applying Bejan method to these systems. Moreover, the study published by Neveu et al. [18] proposes an expression to evaluate the mean thermal power of the reactor, based on exergy balance:

$$\dot{q} = \bar{\theta} / Z \quad (7)$$

where  $\bar{\theta} = 1 - T_0/\bar{T}$

$T_0$ : temperature applied to the left side of the fin (K)  
 $\bar{T}$ : mean temperature of the reactive material (K).

However, nor experimental neither computational validations are yet available. Such validation is still required.

### 3. Materials and methods

The starting point of the present work has been briefly described in section 2.1 and is deeply explained by Verdier et al. [8]. The TES system is a parallel fins heat exchanger (Fig. 2), which geometry slightly differs from the one related to the ptv problem (Fig. 4a), since heat is supplied to the PCM through the fins and through the sole of the heat exchanger. That defines the 'surface to volume' problem (stv) (Fig. 4b). In the ptv problem, heat is supplied only on the left part of the fin, while in the stv problem the heat is

supplied through the left layer (see Fig. 4). In both cases, constant temperature  $T_0$  is taken as boundary condition (red arrows).

The assumptions firstly stated by Bejan [25], used by Tescari [29] and Neveu [31] are:

- The active material (here the PCM) is characterized by the thermal conductivity  $k_a$  and a uniform and constant heat source  $\sigma_q$  ( $\text{Wm}^{-3}$ )
- The conductive material (here copper) is characterized by the thermal conductivity  $k_c$

For the ptv problem, 1D heat transfer is assumed (slenderness assumption), following H-direction in the active material, L-direction in the conductive fin. Under these assumptions, exergy impedance and optimal shape factor are given by Eqs. (5) and (6) derived by Tescari [29].

For the stv problem, these two quantities are derived in the present paper in sub-section 3.1. The optimal configurations for both 'point to volume' and 'surface to volume' problems are then tested, numerically, based on Calvet et al. model [32] and using a CFD software (Comsol®). 2D modelling principles are recalled in sub-section 3.2.

#### 3.1. Impedance minimization method for stv problem

To extend the impedance model to stv problem, let's first notice that an equivalent electrical circuit can be associated to the ptv problem. From Equations (3) and (7), it consists in a perfect current source  $q$  charging the impedance  $Z_0$  (Fig. 5a).

Comparing Fig. 4a and b, the 'surface to volume' problem could be seen as the association of two impedances in parallel (Fig. 5b),  $Z_0$  related to the 'point to volume' problem and  $Z_1$  related to a system consisting only on PCM material and receiving heat from its left side (Fig. 6a).

Similar system has been already analysed in Tescari's work [29] when the entropy production  $S_{irr}$  occurring in the active material is derived. For the system represented in Fig. 6b, this latter writes (Eq. (11) from Ref. [29]):

$$\dot{S}_{irr} = \frac{WX\sigma_q^2}{3k_a T_0^2} Y^3 \quad (8)$$

Thence, the total entropy production  $S_1$  of the system represented in Fig. 6a can be simply obtained by substituting  $Y$  by  $L$  and  $X$  by  $(H-d)$  in Eq. (8):

$$\dot{S}_1 = \frac{W(H-d)\sigma_q^2}{3k_a T_0^2} L^3 \quad (9)$$

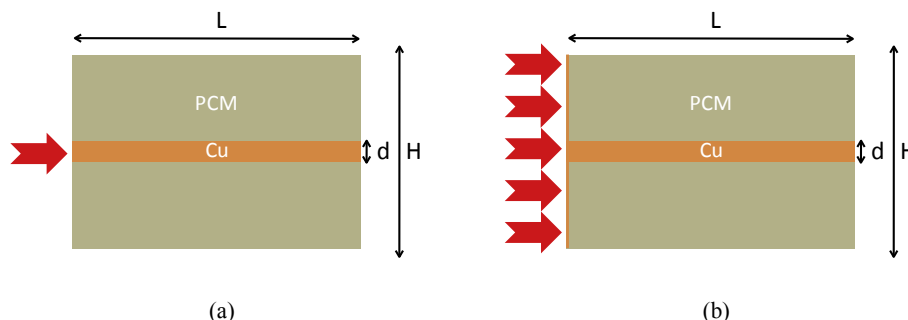


Fig. 4. (a) 'Point to volume' problem, (b) 'Surface to volume' problem.

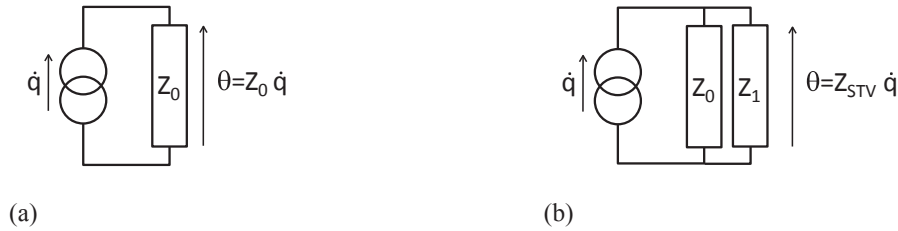


Fig. 5. Equivalent electrical circuit. (a) 'Point to volume' problem. (b) 'Surface to volume' problem.

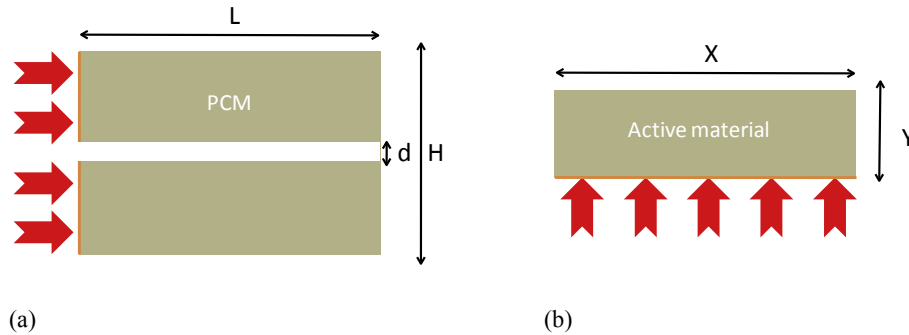


Fig. 6. (a) Complementary system for  $Z_1$  evaluation. (b) System analysed by Tescari [29].

which can be rearranged in:

$$\dot{S}_1 = \frac{\overbrace{\dot{Q}^2}^{W^2(H-d)^2 L^2 \sigma_q^2}}{3k_a T_0^2} \frac{L}{W(H-d)} \quad (10)$$

Remarking that the total heat generated by the active material writes:

$$\dot{Q} = W(H-d)L\sigma_q \quad (11)$$

It yields:

$$\dot{S}_1 = \frac{1}{3k_c W T_0^2} \frac{\tilde{k}}{f(1-\phi)} \dot{Q}^2 \quad (12)$$

Thence, exergy destruction writes:

$$ex_d = T_0 \dot{S}_1 = \frac{1}{3k_c W T_0} \frac{\tilde{k}}{f(1-\phi)} \dot{Q}^2 \quad (13)$$

which gives the exergy impedance  $Z_1$ :

$$Z_1 = \frac{1}{3k_c W T_0} \frac{\tilde{k}}{f(1-\phi)} \quad (14)$$

The impedance related to the 'surface to volume' flow problem is then:

$$Z_{stv} = \left( \frac{1}{Z_0} + \frac{1}{Z_1} \right)^{-1} \quad (15)$$

From Eqs. (14) and (4), we get:

$$Z_{stv} = \frac{1}{3k_c W T_0} \frac{\tilde{k}}{\tilde{f}} \left( 1 - \phi + \frac{\tilde{k}\phi}{1 + \left(\frac{\tilde{f}}{f_0^*}\right)^2} \right)^{-1} \quad (16)$$

or, in dimensionless form:

$$z_{stv} = \frac{\tilde{k}}{\tilde{f}} \left( 1 - \phi + \frac{\tilde{k}\phi}{1 + \left(\frac{\tilde{f}}{f_0^*}\right)^2} \right)^{-1} \quad (17)$$

where  $f_0^*$  is the optimal shape factor related to the 'point to volume' flow problem, given by Eq. (6). The impedance  $z_{stv}$  presents two extrema, given by the roots of:

$$\frac{\partial z_{stv}}{\partial \tilde{f}} = 0 \quad (18)$$

It is found:

$$\begin{aligned} f_1^* &= f_0^* \left[ \frac{\alpha - 2 + (\alpha^2 - 8\alpha)^{1/2}}{2} \right]^{1/2} f_2^* \\ &= f_0^* \left[ \frac{\alpha - 2 - (\alpha^2 - 8\alpha)^{1/2}}{2} \right]^{1/2} \end{aligned} \quad (19)$$

with  $\alpha = \frac{\tilde{k}\phi}{1-\phi}$

Fig. 7 presents the evolution of dimensionless admittance ( $1/z$ ) as a function of the shape factor, related to the ptv ( $z_0$ ) and stv ( $z_1$  and  $z_{stv}$ ) problems. The values of  $\phi$  and  $\tilde{k}$  correspond to the experimental set-up depicted in section 3.1. For ptv problem, optimal shape factor is  $f_0^* = 0.56$ . For stv problem,  $f_2^*$  corresponds to a local maximum ( $f_2^* = 0.65$ ) and  $f_1^*$  to the local minimum ( $f_1^* = 1.96$ ) of conductance (i.e. local minimum and local maximum for impedance). Thence, the optimal shape is given by  $f_2^*$ .

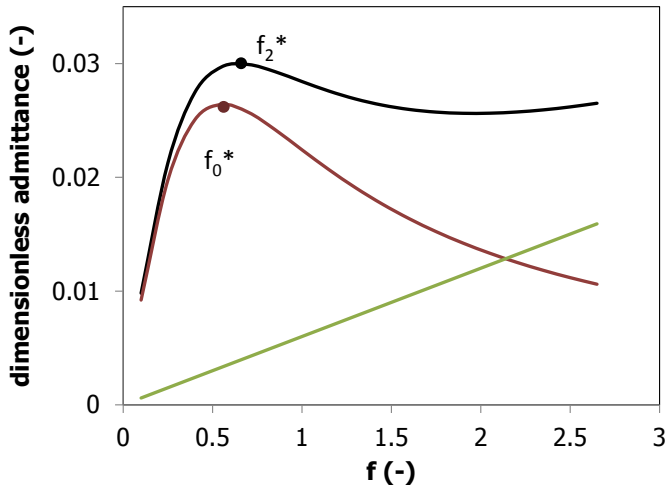


Fig. 7. Dimensionless admittance vs shape factor.  $\phi = 0.0951$ ,  $\bar{k} = 150.7$ . Where - black:  $1/z_{stv}$ , - red:  $1/z_0$ , - green:  $1/z_1$ . (For interpretation of the references to colour in this figure legend, the reader is referred to the web version of this article.)

### 3.2. 2D Model

A 2D transient model has been developed by Comsol® 4.3b simulating the PCM tank described in Ref. [9] and Section 3.1, to validate the developed methodology. The tank is a fin heat exchanger, composed by copper and PCM,  $\text{Li}_2\text{CO}_3$  which melts and solidifies at  $723^\circ\text{C}$ . The heat equations used to describe the system are Eq. (20) for the copper fin and Eq. (21) for the PCM,  $\sigma_q$  being the heat source ( $\text{W}\cdot\text{m}^{-3}$ ), expressed by Eq. (22), which depends on the latent heat ( $L_m$  ( $\text{J}\cdot\text{kg}^{-1}$ )) and the evolution of the fraction of liquid,  $\phi$ . Heating (melting) process is considered:

$$\rho_{Cu} c_{Cu} \frac{\partial T}{\partial t} = \nabla(k_{Cu} \nabla T) \quad (20)$$

$$\rho_{PCM} c_{PCM} \frac{\partial T}{\partial t} = \nabla(k_{PCM} \nabla T) + \sigma_q \quad (21)$$

$$\sigma_q = -\rho L_m \frac{\partial \phi}{\partial t} \quad (22)$$

where:  $\rho$  is the density ( $\text{kg}\cdot\text{m}^{-3}$ ),  $c$  is the specific thermal capacity ( $\text{J}\cdot\text{kg}^{-1}\cdot\text{K}^{-1}$ ),  $k$  is the thermal conductivity ( $\text{W}\cdot\text{m}^{-1}\cdot\text{K}^{-1}$ ), and  $T$  is the temperature (K).

The evolution of the liquid fraction can be written as an ordinary differential equation (ODE), following the simplified phase field method described in Section 2.1:

$$\frac{d\phi}{dt} = \beta(T - T_m)(1 - \phi) \quad (23)$$

where  $\beta$  is a constant set at  $0.001 \text{ K}^{-1}\cdot\text{s}^{-1}$ , fitted from experimental results [9], and  $T_m$  is the melting temperature (K). All the material properties, of both copper and PCM, are listed in Table 1.

The initial and boundary conditions are:

- $t = 0$ , uniform initial temperature:  $T_{Cu} = T_{PCM} = 973 \text{ K}$ ,  $\phi = 0$
- $x = L$  or  $y = \pm H/2$ : perfect insulation:  $\nabla T \cdot \mathbf{n} = 0$

For  $x = 0$ , the boundary conditions depends on the problem. For ptv problem (Fig. 4a), uniform temperature  $T_0 = 1173 \text{ K}$  is imposed for  $-d/2 < y < d/2$ , and perfect insulation is assumed elsewhere. For stv problem (Fig. 4b), uniform temperature  $T_0 = 1173 \text{ K}$  is imposed

Table 1

Material properties of copper and PCM, adapted from Ref. [9].

Properties	Copper	$\text{Li}_2\text{CO}_3$	
		Solid	Liquid
Density, $\rho$ , ( $\text{kg}\cdot\text{m}^{-3}$ )	8940	2110	2110
Thermal conductivity, $k$ , ( $\text{W}\cdot\text{m}^{-1}\cdot\text{K}^{-1}$ )	392	2.6	2.6
Heat capacity, $c$ , ( $\text{J}\cdot\text{kg}^{-1}\cdot\text{K}^{-1}$ )	385	1800	2500
Latent heat, $L_m$ , ( $\text{J}\cdot\text{kg}^{-1}$ )	n.a.	509	
Melting temperature, $T_m$ , (K)	1403	996	

on the whole left edge.

Thanks to the symmetry of the systems, only half of the elemental volume is modelled ( $0 < y < H/2$ ), with a symmetry boundary condition in  $x = 0$  ( $\nabla T \cdot \mathbf{n} = 0$ ).

## 4. Results and discussion

To compare the results of both ‘point to volume’ and ‘surface to volume’ methodologies and seeking for the shape factor giving the best results, the required time ( $t_X$ ) and average heat flux  $\bar{q}_X$  to reach a given global liquid fraction  $X$  have been evaluated. The global liquid fraction writes:

$$X(t) = \frac{\iiint_{V_{PCM}} \phi(t) dv}{V_{PCM}} \quad (24)$$

Then, the evolution of the global liquid fraction versus time can be evaluated for each shape factor, the volumes of PCM and copper being kept constant. As an example, Fig. 8 shows the evolution of the global liquid fraction for ptv problem for three different shape factors. From these evaluations, as in Fig. 8, it can be easily seen which shape factor provides the best geometry leading to the fastest melting of the PCM.

In addition, the evolution of local liquid fraction versus temperature at several times is also obtained, from where it can be easily seen the status of the phase change of each point (this is shown in section 4.2).

The average heat flux to reach  $X$  is:

$$\bar{q}_X = \frac{1}{t_X} \int_0^{t_X} \left( \iint_{S_0} \mathbf{j}_q ds \right) dt \quad (25)$$

where  $S_0$  is the heated surface in  $\text{m}^2$ , and  $\mathbf{j}_q$  the heat flux density crossing this surface in  $\text{Wm}^{-2}$ .

Due to accuracy problems when  $X$  reaches high values (i.e. very slow evolution when  $X$  is close to 1, see Fig. 8),  $t_X$  and  $\bar{q}_X$  were estimated for  $X = 0.9$ . First, the time  $t_{X=0.9}$  is searched such as:

$$\iiint_{V_{PCM}} \phi(t_{0.9}) dv = 0.9 \quad (26)$$

Thence, the average heat flux is determined with:

$$\bar{q}_{0.9} = \frac{1}{t_{X=0.9}} \int_0^{t_{0.9}} \left( \iint_{S_0} \mathbf{j}_q ds \right) dt \quad (27)$$

### 4.1. ‘Point to volume’ problem

The time needed to reach a 90% liquid fraction for each shape factor is shown in Fig. 9. The obtained results follow a curve giving a minimum which leads to the optimum shape factor. The shape factor of 0.56 gives the lowest time, being 12480 s, which corroborates the one previously deduced from impedance minimization

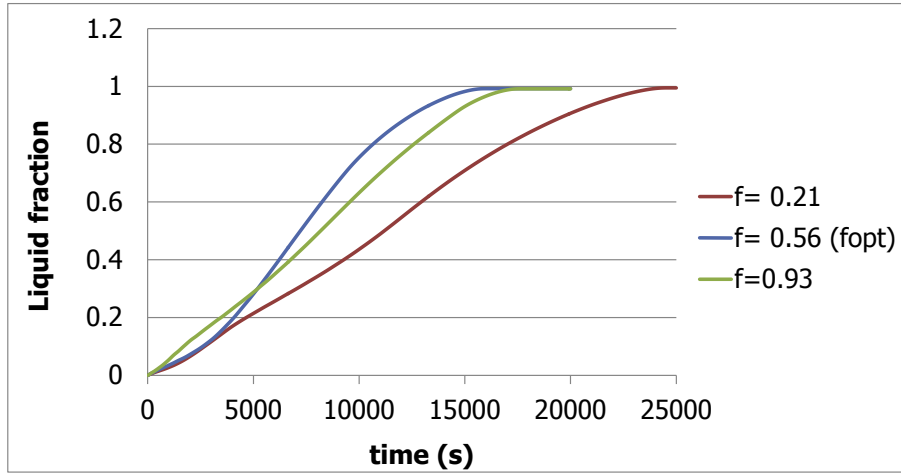


Fig. 8. Liquid fraction as a function of time for three different shape factor (ptv problem).

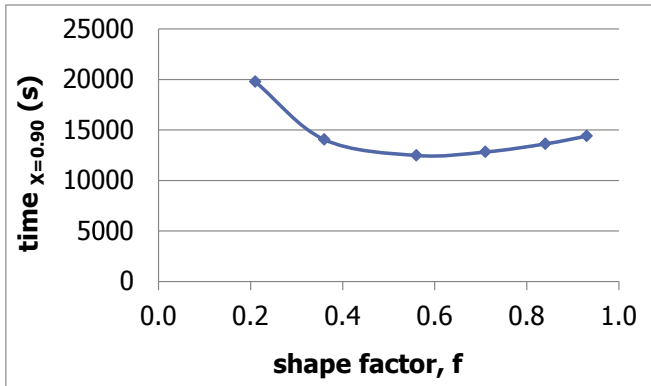


Fig. 9. Time to achieve 90% of liquid fraction as a function of shape factor.

(see eq. (6) and section 3.1).

The average heat flux  $\bar{q}_{0.9}$  (Eq. (27)) is plotted in Fig. 10 as a function of the shape factor ( $f$ ), and compared with the one deduced from Eq. (7) taking the melting temperature as equilibrium temperature. Although Eq. (5) underestimates the average heat flux, it can be seen that this expression gives a quite good approximation of the simulated heat power. The 2D model results evaluating the heat flux are 11% higher than the ones following

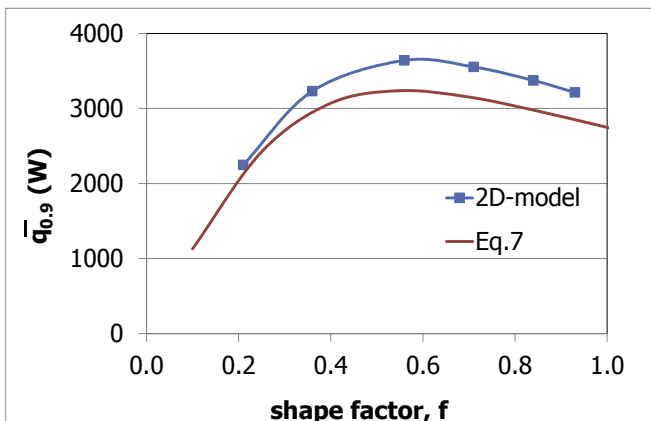


Fig. 10. Average heat flux as a function of shape factor.  $W = 1 \text{ m}$ ,  $\phi = 0.0951$ ,  $\kappa = 150.7$ .

Equation (7) at the optimum shape factor.

The shape factor of the heat exchanger presented in Ref. [9] and in Fig. 2 corresponds to a shape factor of 0.21, which leads to higher time to reach the same percentage of liquid fraction and consequently lower values of heat flux, compared to the other shape factors. The results of the studied heat exchanger show that its optimization can lead to remarkable savings of melting time of around 36%. Of course, this also corroborates that the built heat exchanger was not the optimum and has to be refined.

#### 4.2. 'Surface to volume' problem

In the case that the entire bottom layer is heated (stv problem), the curve presents a minimum and a maximum (see Eq. (19)), and both are corroborated by the model results as it can be observed in Figs. 11 and 12.

The shape factor giving a minimum impedance (see Section 3.1) is  $f_2^* = 0.65$ . The 2D model results show that the optimum shape factor, giving the lowest time and highest heat flux values, is around 0.7. This can be observed in Figs. 11 and 12, respectively. Results show that the time to reach a 90% of melted PCM is 11900 s (see Fig. 11). Regarding Fig. 12, the 2D model is in agreement with impedance minimization method (Eq. (7)), showing differences of the heat flux at the optimum shape factor of around 8%.

On the other hand, the shape factor  $f_1$  leading to local maximum impedance (see Section 3.1) is around 1.5 according to the model

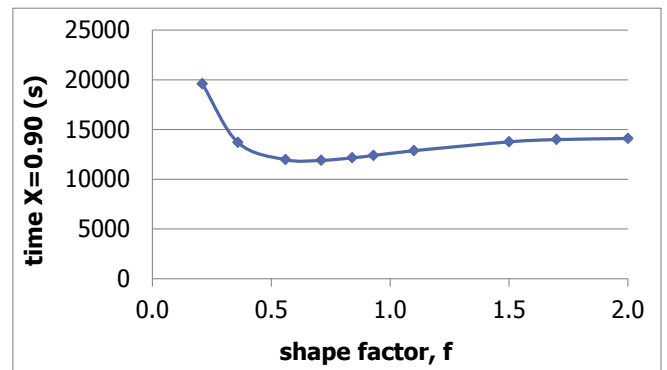


Fig. 11. Time to achieve 90% of liquid fraction as a function of shape factor.  $\phi = 0.0951$ ,  $\kappa = 150.7$ .

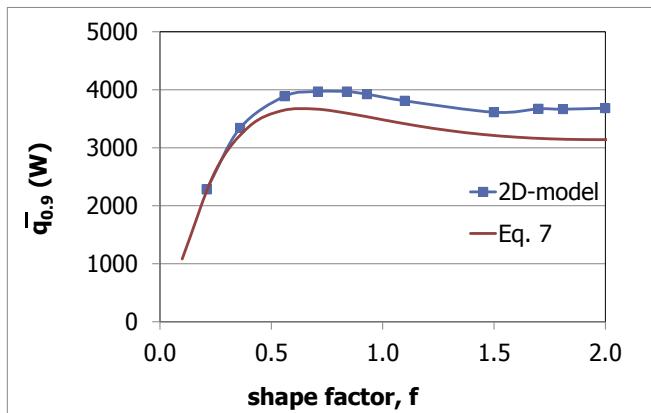


Fig. 12. Heat flux average as a function of shape factor,  $W = 1$  m,  $\phi = 0.0951$ ,  $\bar{\kappa} = 150.7$ .

(Fig. 12), although Eq. (19) gives 1.96 for  $f_1^*$ . The difference is considerable, but could be explained by the fact that the slenderness assumption used in the impedance calculation is no more valid for high  $f$  value.

When comparing both optimums for ptv and stv problems, it can be noticed that stv configuration leads to an expected faster melting process, of around 10 min, and 330 W higher heat flux value. This behaviour was expected since in ptv problem, heat is supplied only on the left part of the fin, while in the stv problem all the heat is supplied through the left layer (see Fig. 4). Nevertheless, this is the first time that impedance minimization methodology is developed for a stv configuration and numerically demonstrated. The results out from this study corroborate not only the expected faster melting process with stv configuration but also that impedance minimization approach can be also implemented for stv configurations.

In addition, it is important to point out that the optimum shape factor for stv problems has shift to higher values meaning lower length and higher height of the system compared to ptv geometry.

The transient 2D model permits to simulate the temperature and liquid fraction field according to time. Such fields evolution are presented in Figs. 13 and 14 for two shape factors,  $f = 0.21$ ,

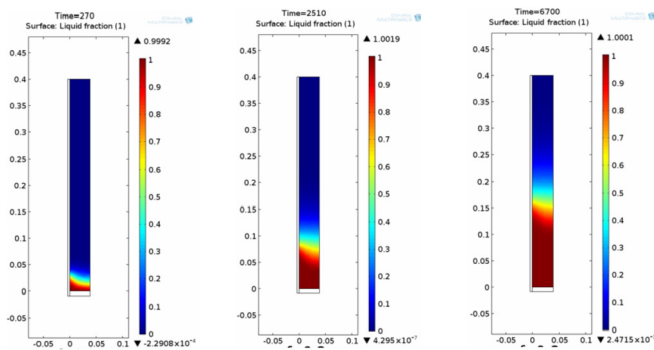


Fig. 13. Evolution of the liquid fraction vs. time for the stv problem when  $f = 0.21$ .

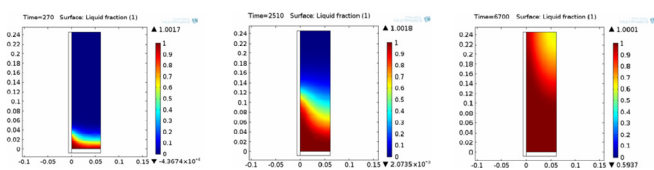


Fig. 14. Evolution of the liquid fraction vs. time for the stv problem when  $f = 0.56$ .

corresponding to the original design experimented by Verdier et al. [9], and  $f = f_0^* = 0.56$  (ptv problem) deduced from the impedance minimization by Eq. (6). It is important to remind that the total volume (surface) is equal for both presented case (i.e. same amount of PCM and copper). It could be immediately seen that the liquid fraction evolution runs faster for the minimal impedance case.

## 5. Conclusions

A 2D model of an elemental volume of a PCM and fins heat exchanger for the ‘point to volume’ case has been developed with Comsol<sup>®</sup> software. The impedance minimization method for ‘point to volume’ problem has been numerically validated by comparing it with the model results. The optimal shape factor found for the studied TES PCM based described system is around 0.56.

The impedance minimization method has been extended for ‘surface to volume’ problem. The ‘surface to volume’ problem 2D model has been developed and demonstrated that the calculated optimum by impedance minimization approach is the one expected, being 0.65, for the same solar receiver application. Stv configuration leads to faster melting process, of around 10 min, and 330 W higher heat flux value when compared to ptv case. Refining the TES system with the stv optimum shape factor would increase the power by 200% compared to the initial non-optimized configuration.

Therefore, it can be concluded that the impedance minimization approach is a useful and powerful method to start a PCM storage tank optimization for both ‘point to volume’ or ‘surface to volume’ problems. The obtained optimum geometry by this method is completely in agreement with the developed 2D model results simulating a PCM and fin heat exchanger by Comsol<sup>®</sup> multiphysics software.

Further work is planned, for instance to perform the experimental tests to validate the model and adjust some parameters, to compare the presented 2D model with another more complex and presented in Ref. [34], and to extend the model for sensible and TCM systems.

## Acknowledgements

The author Aran Solé would like to thank the Societat Econòmica Barcelonesa Amics del País (SEBAP) for the funds that made possible her research stay. The authors would like to thank Jean-Marie Mancaux for his help and Jinqiu Shen for her contribution in the work. The authors would like to thank the Catalan Government for the quality accreditation given to their research group GREA (2014 SGR 123). GREA is certified agent TECNIO in the category of technology developers from the Government of Catalonia. The work is partially funded by the Spanish government (ENE2015-64117-C5-1-R (MINECO/FEDER)). The research leading to these results has received funding from the European Union’s Horizon 2020 research and innovation programme under grant agreement No 657466 (INPATH-TES). Aran Solé would like to thank Ministerio de Economía y Competitividad de España for Grant Juan de la Cierva, FJCI-2015-25741.

## References

- [1] Worldwide trends in energy use and efficiency, Key Insights from IEA Indicator Analysis, International Energy Agency, 2008. [https://www.iea.org/publications/freepublications/publication/Indicators\\_2008.pdf](https://www.iea.org/publications/freepublications/publication/Indicators_2008.pdf).
- [2] Technology Roadmap, Concentrating Solar Power, International Energy Agency, 2010, <https://doi.org/10.1787/9789264088139-en>.
- [3] M.J. Vassallo, J.M. Bravo, A MPC approach for optimal generation scheduling in CSP plants, *Appl. Energy* 165 (2016) 357–370.
- [4] X. Py, Y. Azoumah, R. Olives, Concentrated solar power: current technologies, major innovative issues and applicability to West African countries, *Renew.*

- Sustain. Energy Rev. 18 (2013) 306–315.
- [5] K. Lovegrove, M. Watt, R. Passey, G. Pollock, J. Wyder, J. Dowse, Realising the Potential of Concentrating Solar Power in Australia: Summary for Stakeholders, Australian Solar Institute Pty, Limited, 2012.
  - [6] A. Gil, M. Medrano, I. Martorell, A. Lázaro, P. Dolado, B. Zalba, L.F. Cabeza, State of the art on high temperature thermal energy storage for power generation. Part 1—concepts, materials and modellization, *Renew. Sustain. Energy Rev.* 14 (1) (2010) 31–55.
  - [7] M. Liu, J.C. Gomez, C.S. Turchi, N.H.S. Tay, W. Saman, F. Bruno, Determination of thermo-physical properties and stability testing of high-temperature phase-change materials for CSP applications, *Sol. Energy Mater. Sol. Cells* 139 (2015) 81–87.
  - [8] D. Verdier, Q. Falcoz, A. Ferrière, Design of a protection thermal energy storage using phase change material coupled to a solar receiver, *High Temp. Mater. Process.* 33 (6) (2014) 509–523.
  - [9] D. Verdier, A. Ferrière, Q. Falcoz, F. Siro, R. Couturier, Experimentation of a high temperature thermal energy storage prototype using phase change materials for the thermal protection of a pressurized air solar receiver. SolarPACES 2013, *Energy Proc.* 49 (2014) 1044–1053.
  - [10] G. Peiro, J. Gasia, L. Miro, C. Prieto, L.F. Cabeza, Experimental analysis of charging and discharging processes with parallel and counter flow arrangements, in a molten salts high temperature pilot plant scale setup, *Appl. Energy* 178 (2016) 394–403.
  - [11] E. Koepf, W. Villasmil, A. Meier, Pilot-scale solar reactor operation and characterization for fuel production via the Zn/ZnO thermochemical cycle, *Appl. Energy* 165 (2016) 1004–1023.
  - [12] C. Prieto, P. Cooper, A.I. Fernández, L.F. Cabeza, Review of technology: thermochemical energy storage for concentrated solar power plants, *Renew. Sustain. Energy Rev.* 60 (2016) 909–929.
  - [13] S.S.M. Tehrani, R.A. Taylor, P. Saberi, G. Diarce, Design and feasibility of high temperature shell and tube latent heat thermal energy storage system for solar thermal power plants, *Renew. Energy* 96 (2016) 120–136.
  - [14] B. Xu, P. Li, C. Chan, Application of phase change materials for thermal energy storage in concentrated solar thermal power plants: a review to recent development, *Appl. Energy* 160 (2015) 286–307.
  - [15] M. Wu, C. Xu, Y.-L. He, Dynamic thermal performance analysis of a molten-salt packed-bed thermal energy storage system using PCM capsules, *Appl. Energy* 121 (2014) 184–195.
  - [16] P.A. Galione, C.D. Pérez-Segarra, I. Rodríguez, A. Oliva, J. Rigola, Multi-layered solid-PCM thermocline thermal storage concept for CSP plants. Numerical analysis and perspectives, *Appl. Energy* 142 (15) (2015) 337–351.
  - [17] B.-C. Zhao, M.-S. Cheng, C. Liu, Z.-M. Dai, Thermal performance and cost analysis of a multi-layered solid-PCM thermocline thermal energy storage for CSP tower plants, *Appl. Energy* 178 (15) (2016) 784–799.
  - [18] M. Longeon, A. Soupant, J.-F. Fourmigué, A. Bruch, P. Marty, Experimental and numerical study of annular PCM storage in the presence of natural convection, *Appl. Energy* 112 (2013) 175–184.
  - [19] Y.B. Tao, Y.L. He, Numerical study on thermal energy storage performance of phase change material under non-steady-state inlet boundary, *Appl. Energy* 88 (11) (2011) 4172–4179.
  - [20] F. Fornarelli, S.M. Camporeale, B. Fortunato, M. Torresi, P. Oresta, L. Magliocchetti, A. Miliozzi, G. Santo, CFD analysis of melting process in a shell-and-tube latent heat storage for concentrated solar power plants, *Appl. Energy* 164 (2016) 711–722.
  - [21] A. Sciacovelli, F. Gagliardi, V. Verda, Maximization of performance of a PCM latent heat storage system with innovative fins, *Appl. Energy* 137 (2015) 707–715.
  - [22] C. Zauner, F. Hengstberger, M. Etzel, D. Lager, R. Hofmann, H. Walter, Experimental characterization and simulation of a fin-tube latent heat storage using high density polyethylene as PCM, *Appl. Energy* 179 (2016) 237–246.
  - [23] K. Nithyanandam, R. Pitchumani, Computational studies on a latent thermal energy storage system with integral heat pipes for concentrating solar power, *Appl. Energy* 103 (2013) 400–415.
  - [24] Z. Liu, Y. Yao, H. Wu, Numerical modeling for solid–liquid phase change phenomena in porous media: shell-and-tube type latent heat thermal energy storage, *Appl. Energy* 112 (2013) 1222–1232.
  - [25] A. Bejan, *Shape and Structure, from Engineering to Nature*, Cambridge University Press, Cambridge, England, 2000.
  - [26] K. Manjunath, S.C. Kaushik, Second law of thermodynamic study of heat exchangers: a review, *Renew. Sustain. Energy Rev.* 40 (2014) 348–374.
  - [27] Y. Azoumah, N. Mazet, P. Neveu, Constructal network for heat and mass transfer in a solid–gas reactive porous medium, *Int. J. Heat Mass Tran.* 47 (14–16) (2004) 2961–2970.
  - [28] Y. Azoumah, P. Neveu, N. Mazet, Constructal design combined with entropy generation minimization for solid–gas reactors, *Int. J. Therm. Sci.* 45 (7) (2006) 716–728.
  - [29] S. Tescari, N. Mazet, P. Neveu, Constructal theory through thermodynamics of irreversible processes framework, *Energy Convers. Manag.* 52 (2011) 3176–3188.
  - [30] A. Bejan, Constructal-theory network of conducting paths for cooling a heat generating volume, *Int. J. Heat Mass Tran.* 40 (4) (1997) 799–816.
  - [31] P. Neveu, S. Tescari, D. Aussel, N. Mazet, Combined constructal and exergy optimization of thermochemical reactors for high temperature heat storage, *Energy Convers. Manag.* 71 (2013) 186–198.
  - [32] N. Calvet, X. Py, R. Olivès, J.-P. Bédécarrats, J.-P. Dumas, F. Jay, Enhanced performances of macro-encapsulated phase change materials (PCMs) by intensification of the internal effective thermal conductivity, *Energy* 55 (2013) 956–964.
  - [33] D. Verdier, *Stockage thermique de protection à chaleur latente intégré à un récepteur solaire à air pressurisé*, PhD thesis, Université de Perpignan Via Domitia, <https://hal.archives-ouvertes.fr/tel-01315613>.
  - [34] R. Olivès, X. Py, Q. Falcoz, P. Neveu, J.-M. Mancaux, Intensification des transferts thermiques dans un module de stockage thermique: suivi du front de fusion par thermographie et simulation numérique, in: Conference Paper, SFT 2014, Lyon, 3–6 June, 2014.